Scientific Research Publishing

International Journal of Geosciences, 2022, 13, 281-302
https://www.scirp.org/journal/ijg
ISSN Online: 2156-8367
ISSN Print: 2156-8359

The Potential of Quartzitic Veins in SW Cameroon for High-Purity Quartz

Ngambu Aloysius Afahnwie[1], Arnold Chi Kedia[2*], Cheo Emmanuel Suh[1,2], Cyrille Sigue[2], Elisha Mutum Shemang[3]

[1]Department of Geology, Mining, and Environmental Science, Faculty of Science, University of Bamenda, Bamenda, Cameroon
[2]Economic Geology Unit, Department of Geology, University of Buea, Buea, Cameroon
[3]Department of Earth and Environmental Sciences, Botswana International University of Science and Technology, Palapye, Botswana
Email: *kenardu@yahoo.com

How to cite this paper: Afahnwie, N.A., Kedia, A.C., Suh, C.E., Sigue, C. and Shemang, E.M. (2022) The Potential of Quartzitic Veins in SW Cameroon for High-Purity Quartz. *International Journal of Geosciences*, **13**, 281-302.
https://doi.org/10.4236/ijg.2022.134015

Received: March 15, 2022
Accepted: April 21, 2022
Published: April 24, 2022

Abstract

High-purity quartz (HPQ), the prime source of silica, is increasingly considered a strategic mineral in the world market because it is the raw material for special applications in high-tech industries owing to its unique physical and chemical properties. The expected growth in demand for HPQ implies that more sources have to be found. This is the primary motivation for this study which targets the Supe area, SW Region of Cameroon. The structural occurrences of quartz veins were mapped and samples collected. The chemical nature and textural features of these samples were subsequently analyzed by X-ray tomography, scanning electron microscopy (SEM), and electron microprobe analysis (EMPA). Three deformation events, D_1 - D_3 are recorded. D_1 is marked by the development of the strong S_1 foliation defined by the gneissic layering and schistosity. D_2 is a NE-SW ductile to brittle sinistral shear that controlled the formation of tension gashes that served as subsequent pathways for quartz-rich hydrothermal fluids to circulate and eventually precipitate quartz. The presence of rutile, tourmaline, and mica inclusions in the Supe veins affects the purity of the quartz. However, quartz can be treated to improve its quality. Taking into consideration the nine determinant trace elements used to classify HPQ, three (Li, P, and B) are below detection limits, Al concentrations are within the HPQ, quartz market standard, and average natural abundance; Ti values are high above all three standards in all except one sample, while Na, Ca, K, and Fe values fluctuate, thus classifying one of the samples as high purity quartz and the others as low purity quartz. These veins define tension gashes which usually occur in an echelon arrangement covering a large surface area, suggesting that more of such veins probably exist in the Supe area. Consequently, the quality and potential quantity of HPQ veins in this area suggest a high potential for HPQ exploration in the region.

Keywords

Quartz Veins, High Purity Quartz, X-Ray Tomography, Rutile, Tourmaline

1. Introduction

Quartz is increasingly considered a strategic mineral in the world market because it represents the raw material for special applications in high-tech industries [1]. High purity quartz (HPQ) is the prime source of silica and it has a vast range of applications: in the production of metallurgical silicon, used in the manufacturing of solar panels, specialty chemicals, special filaments, breast and tissue implants, and other optical applications including fiber optics [1] [2] [3].

HPQ is often thought of as a relatively easily available commodity but it is very rare in economic and near-economic quantities. Most deposits around the world occur in quartz-rich granitic pegmatite and hydrothermal quartz veins [4] [5]. However, very few deposits are suitable in volume, quality, and amenability to tailored refining methods for specialty high purity applications (the Purs Pine Deposit North Carolina USA) [2]. The demand for HPQ is increasing strongly due to the rapid development and expansion of the HPQ consuming industries [6] [7].

There is a great price margin between low-quality quartz, which costs 15 to 20 US$ per ton, and HPQ which costs 2000 US$ per ton. Quartz is considered to be high purity when it contains < 50 μg per gram of structurally incorporated trace elements [2] [8] [9]. Transformation of raw quartz into refined high-purity products involves several refinement steps which need to be adapted to effectively minimize the specific impurities of the individual raw quartz feed to comply with stringent end-use specifications [6]. Indeed, refining seeks to achieve HPQ with total impurity levels of less than 20 ppm, thereby creating a highly valuable raw material that commands up to 5 EUR/kg [2].

Impurities within quartz crystals (intercrystalline impurities) are the principal control of the quality of quartz, although they can be removed to some extent by processing. Such impurities include lattice-bound trace elements, submicron (<1 μm) inclusions, mineral and fluid micro-inclusions (>1 μm). In addition, intercrystalline impurities may occur along grain boundaries in the form of mineral coatings or micro-crystals.

The commercial concentration requirements for critical elements which are detrimental to the HPQ products vary considerably. Thus, the definition of HPQ from a commercial point of view is based on the concentration limits of elements that interfere with the quality of melted HPQ products, which are predominantly silica and quartz glass products [1]. Classified HPQ is based on the sum of the concentrations of nine elements (Na, K, Li, Al, Ca, Fe, Ti, B, and P) analyzed on quartz crystals (single grain analysis) or processed quartz sand (bulk product analyses) to be <50 μg per gram.

Today, the US-based Unimin Corp./Sibelco still dominates the global high purity quartz market from operations in North Carolina [8]. One of the few alternative suppliers, Norsk Mineral's Norwegian Crystallites, has been producing high purity quartz from its Drag plant in western Norway and several underground and open-pit mines since mid-1996 when the company changed ownership. Potential new entrants into the high purity quartz world market are still under development such as the quartz resource in the Serra de Santa Helena Formation, Brazil [8], and a few more. The size of the worldwide market is estimated at 30,000 tons per year for the 99.99% purity and above material [2] and the present producing mines have an estimated shortfall of about 15,000 tons. There is consequently a need to find new sources of HPQ, especially in sub-Saharan African countries where the use of solar panels is expected to grow exponentially in the not-too-distant future. This, therefore, is the pivotal motivation for this study.

Recently, large quartz veins have been encountered in basement rocks of the Supe area of SW Cameroon [10]. However, the nature of the veins and the purity of the quartz are not well known as this area is still relatively unexplored although earlier attempts to map this region have been reported from the Tombel Graben by [11] and [12] [13]. The present study sets out to characterize rutile/tourmaline-bearing quartz veins in the Pan-African belt of SW Cameroon in the Supe area. This requires napping of quartz veins and their host rocks with emphasis on the structural context, petrography, and their mineral inclusions therein, and investigation of the potentials of extracting HPQ from these veins by EMPA analysis. Understanding the nature of these veins will enhance the regional interpretation of principal stress orientation during polyphase deformation and allow the evaluation of the purity of the quartz and the origin of their mineral inclusions.

2. Geology of the Study Area

The Supe area is part of the Pan-African mobile belt in SW Cameroon (**Figure 1**). This region is part of the Neoproterozoic fold belt (NFB) of Cameroon, a major part of the Neoproterozoic Braziliano belt [14] [15] and it is affected by the Central African Shear Zone (CASZ) of Braziliano/Pan-African age (600 ± 50 Ma), that is a pre-drift extension of the Pernambuco shear zone in NE Brazil [14] [16]. This transcontinental shear zone is a major crustal discontinuity extending from NEBrazil into Cameroon (**Figure 1(a)**).

Movements along the Pan-African structures have created basins such as the Lom Basin [16] and a series of shallow grabens such as the Tombel Graben SE of the Supe area. The Tombel Graben is one of a series of grabens that defines the alternation of horsts and grabens along the Cameroon Volcanic Line (CVL) [17], which is a linear array of numerous volcanic centers and anorogenic complexes [18] [19] [20]. It has been postulated that the linear trend of volcanoes along the CVL is structurally controlled [21] [22] by Braziliano/Pan-African structures

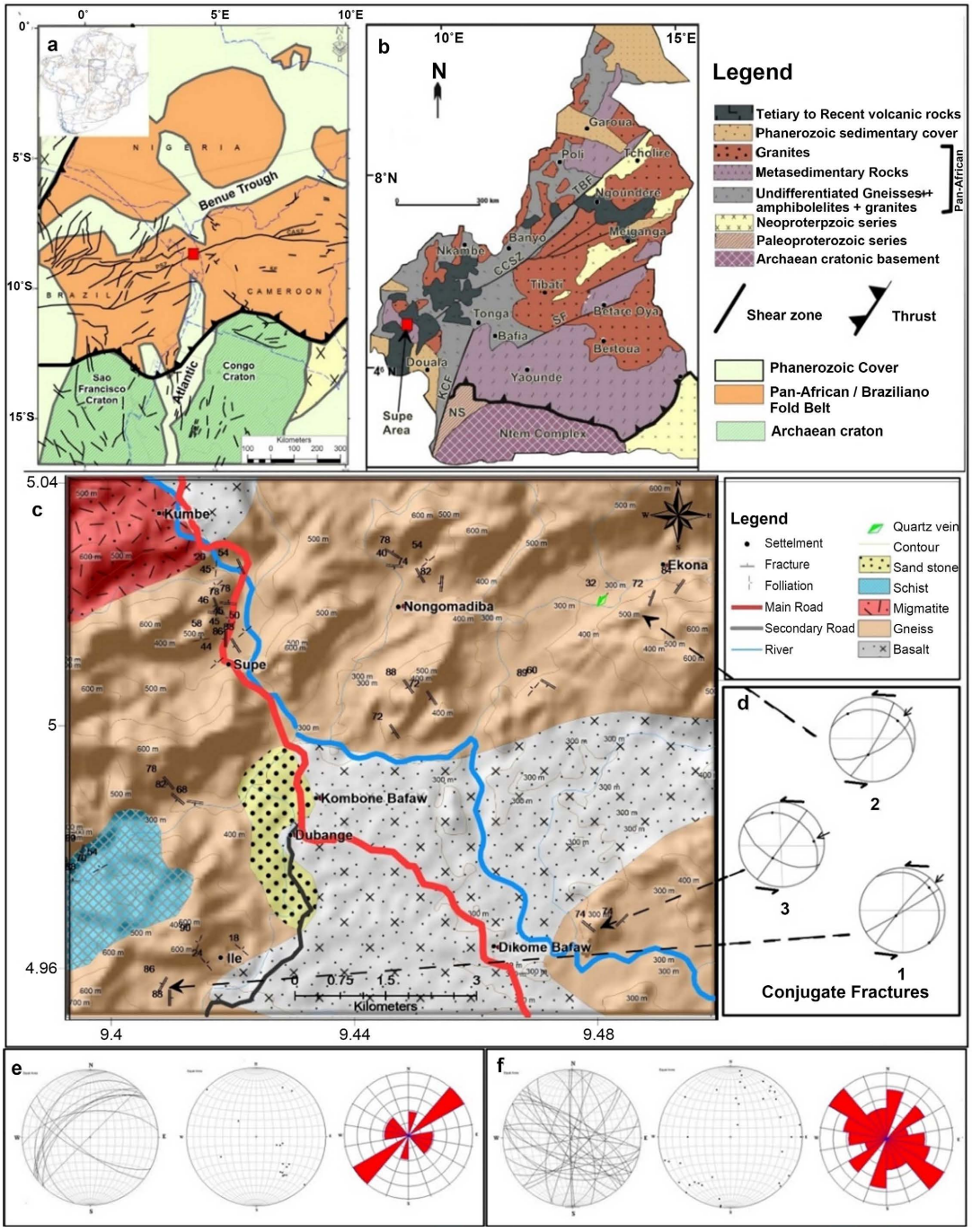

Figure 1. Location of study area (a) Pre-drift reconstruction of Pan-African and Braziliano terraines using Gondwana plates at 141 Ma. CASZ: Central African Shear Zone; SF: Sanaga fault; PF: Patos fault; PSZ: Pernambuco shear zone. The insert shows the fit between Africa and South America at 141 Ma (modified after [24] and [25]. (b) Geologic map of Cameroon showing the Supe area (modified after [26]; BF = Tcholliré-Banyo Fault, SF = Sanaga Fault, KCF = Kribi-Campo Fault. (c) Geologic map for the Supe area with foliations, fractures, and quartz vein attitudes; (d) conjugate fractures showing principal stress directions: 1) Angle = 159.1˚ or 20.90, $\delta 1$ = N49.7, 16.8NE, $\delta 2$ = N233.4, 73.2SW, $\delta 3$ = N140.0, 1.0SE. 2) Angle = 34.5˚ or 145.5˚, $\delta 1$ = N54.0, 26.8N, $\delta 2$ = N197.1, 57.7S, $\delta 3$ = N315.3, 16.6W. 3) Angle = 96.9˚ or 83.1˚, $\delta 1$ = N081.7, 22.1E, $\delta 2$ = N216.0, 59.8S, $\delta 3$ = N343.4, 19.5N, (e) β, Π and rose diagrams of gneissosity and schistosity with a general NE-SW trend, (f) β, Π and rose diagrams for fractures with two dominant fracture trends (NW-SE and NE-SW) for the Supe area.

that predate the onset of volcanism. Indeed, the CVL is affected by a trans-lithosphere fault zone which can be traced to pre-date the opening of the South Atlantic Ocean, in Brazil as the Pernambuco dextral transcurrent fault system [23]. The basement of the continental sector of the CVL is composed of Precambrian and Pan-African age rocks. Syn-tectonic alkaline, granites, crystalline schists, and gneisses with rare syenites, gabbros, and diorites belonging to Pan African Orogeny have been dated as 620 - 480 Ma [23]. These rocks outcrop mostly in the central and NW part of the CVL.

This mobile belt is known to host several mineral deposits of economic importance such as the U-Mo mineralization in the Pan-African granites of the Ekomédion prospect [27] [28], the U mineralization at Kitongo, N Cameroon [29], the detrital rutile in the Yaounde region, the lode gold mineralization at Dimako-Mboscorro, SE Cameroon [30], and the Belikombone hill gold prospect (E) Cameroon [31] and references therein.

Lithologic units of the Supe area are made up of three major rock types: metamorphic rocks that cover ~65% of the area and that are dominated by gneiss, igneous rocks covering ~30% and consisting mainly of basalt, and sedimentary rocks that cover ~5% of the area (**Figure 1(c)**).

The major metamorphic rocks in this area are gneisses, migmatites, and schists. The gneisses are generally light-colored, coarse-grained, and have granoblastic textures. Their main minerals are biotite, muscovite, quartz, and feldspar (alkali feldspars and plagioclase) in various proportions. These minerals are commonly aligned in a parallel manner to each other forming alternating light and dark bands of 0.5 - 1.5 cm thick but occasionally without a clear banding. The migmatites mostly occur in association with gneisses. They are commonly light-colored, and coarse-grained with minerals that include quartz, feldspars, and micas. They are moderately foliated with very thick bands of ~7 cm in the outcrop. The schists encountered here are light-colored with continuous schistosity and they are made up of muscovite, biotite, quartz, and feldspar, which are strongly aligned.

Foliation surfaces (**Figure 2(a)** and **Figure 2(b)**) were mapped in gneisses, schists, and some migmatites. Data from these surface planes were plotted on stereonets (Π diagrams and β diagrams) and on rose diagrams (**Figure 1(d)**) showing that the gneissose, schistose, and migmatitic foliations have a NE-SW general trend between N231E-N240E. Fractures tend to crosscut the foliations at various angles although some are sub-parallel. It appears from the Π, β, and rose diagrams (**Figure 1(e)**) that the fractures have a dominant NW-SE trend between N131E-N140E and a somewhat less pronounced NE-SW trend between N180E-N190E. Microfaults were also encountered (**Figure 2(c)** and **Figure 2(d)**). Some of the fractures are open while others are filled by quartz veins that range from a few cm wide to about 1.5 m and about 35 - 40 m long. Stereographic projections of the conjugate fractures (**Figure 1(f)**) indicate a NE compression in the principal stress directions, δ_1, and a corresponding NW-SE extension direction. Folds in the area have axial planes that generally trend in a NW-SE direction (**Figure 3**).

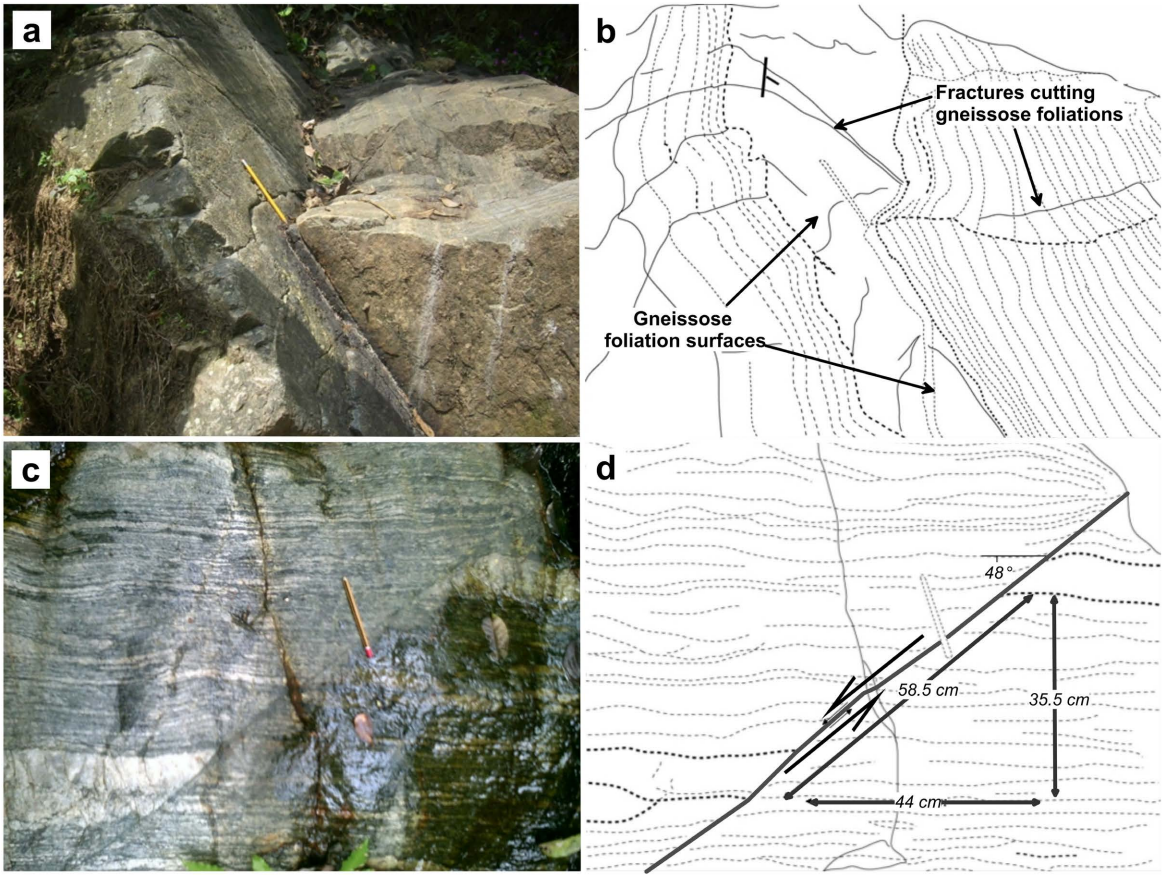

Figure 2. Micro faults in the Supe area. (a) and (b) Gneissosity cut by fractures, (c) and (d) Microfault with a sinistral shear sense.

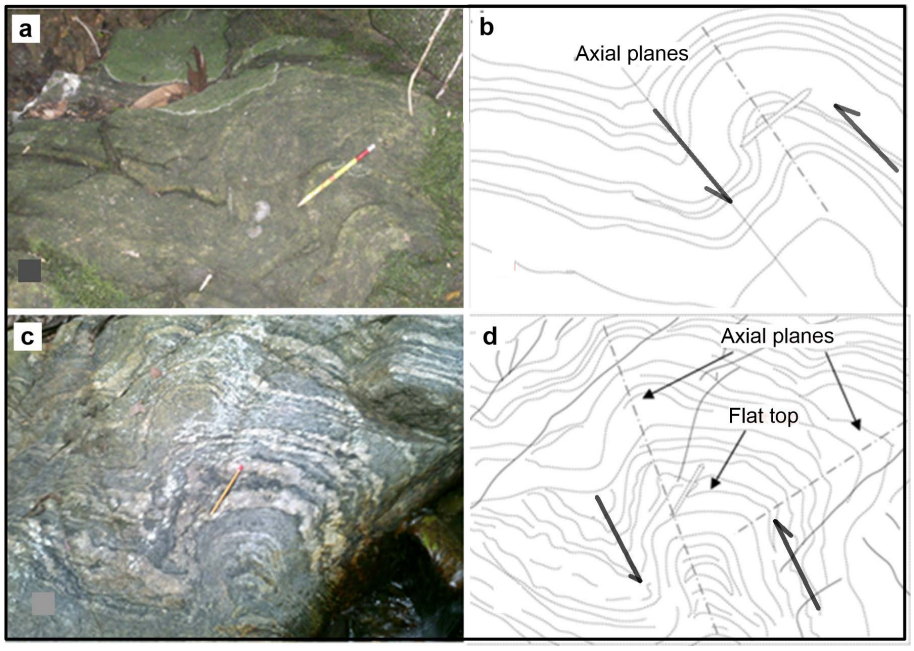

Figure 3. Folds in the Supe area with axial planes trending in a NW-SE direction: (a) and (b) Asymmetric fold showing an inclined axial plane, (c) and (d) Box fold showing a flat top, with 2 inclined axial planes.

Basalts are the dominant igneous rocks of the area (amygdaloidal and porphyritic basalt). They occur as flows (aa and blocky lava) and dyke-like masses with vertical and horizontal columns and joints. However, some dolerites were encountered in the contact with gneisses and migmatites. Granites in the Supe area occur as stock-like masses. They are massive, light-colored with coarse grains and a graphic texture.

Sandstones occur alternating with shales dipping in a NE direction and outcrop along river beds. The shales are dark grey, fine-grained, and fissile. The sandstones are light-colored (whitish) with poorly sorted with variable grain sizes. They are friable with sub-angular grains and minerals such as quartz, orthoclase feldspar, biotite, and muscovite. They have very little cementing material, which is probably calcite or iron oxide.

Structural Occurrence and Texture of Quartz veins

Quartz-rich veins of about 35 - 40 m long and 1 - 1.5 m wide were mapped. They have a NE-SW trend and are lensoid in shape (**Figure 4**). Some of the veins have yellowish quartz grains which are sugary to saccharoidal in texture and thus crumble easily. These crumbly veins have a diverging, ENE-WSW, trend and are dominated by coarser (~4 cm), more compact, and homogeneous white quartz. The quartz crystals range from clear to white with glassy to greasy lusters. Large mineral inclusions such as muscovite flakes, black slender rutile crystals, and dark-blue to black tourmaline needles are common (**Figure 5**). The transition into the gneiss shows a concentration of rutile and tourmaline crystals bound by a quartz matrix-forming porphyritic rutile-rich black tourmaline.

Three deformation events (D_1 - D_3) are recorded by the structures in this. D_1 is marked by the development of the strong S1 foliation defined by the gneissose layering and schistosity. D_2 is a NE-SW ductile to brittle sinistral shear that controlled the formation of tension gashes that served as subsequent pathways for quartz-rich hydrothermal fluids to circulate and eventually precipitate quartz. A D_2 sinistral shear with a distinct Pan-African signature has been reported in the CASZ portion of the Tombelgraben [12] [13] [17] which resulted in a NE-SW mylonitic foliation that is subparallel to the regional trend of the North Equatorial fold belt (NFB) and Braziliano belt. These structural similarities show that the Supe area is also part of the NFB of Cameroon, a significant contribution to the tectonics of this area.

3. Materials and Methods

Representative quartz samples obtained from the veins are white, coarse, compact, and homogeneous. The rock samples were crushed, and selected grains were examined under a binocular microscope, subsequently polished and coated with carbon before SEM imaging and analysis. The polished sections were analyzed using a Quanta 600F scanning electron microscope (SEM). X-ray tomography was applied at the University of Ghent, Belgium, for analysis of the internal features and the nature of the inclusions, following n [32] [33]. Hundreds

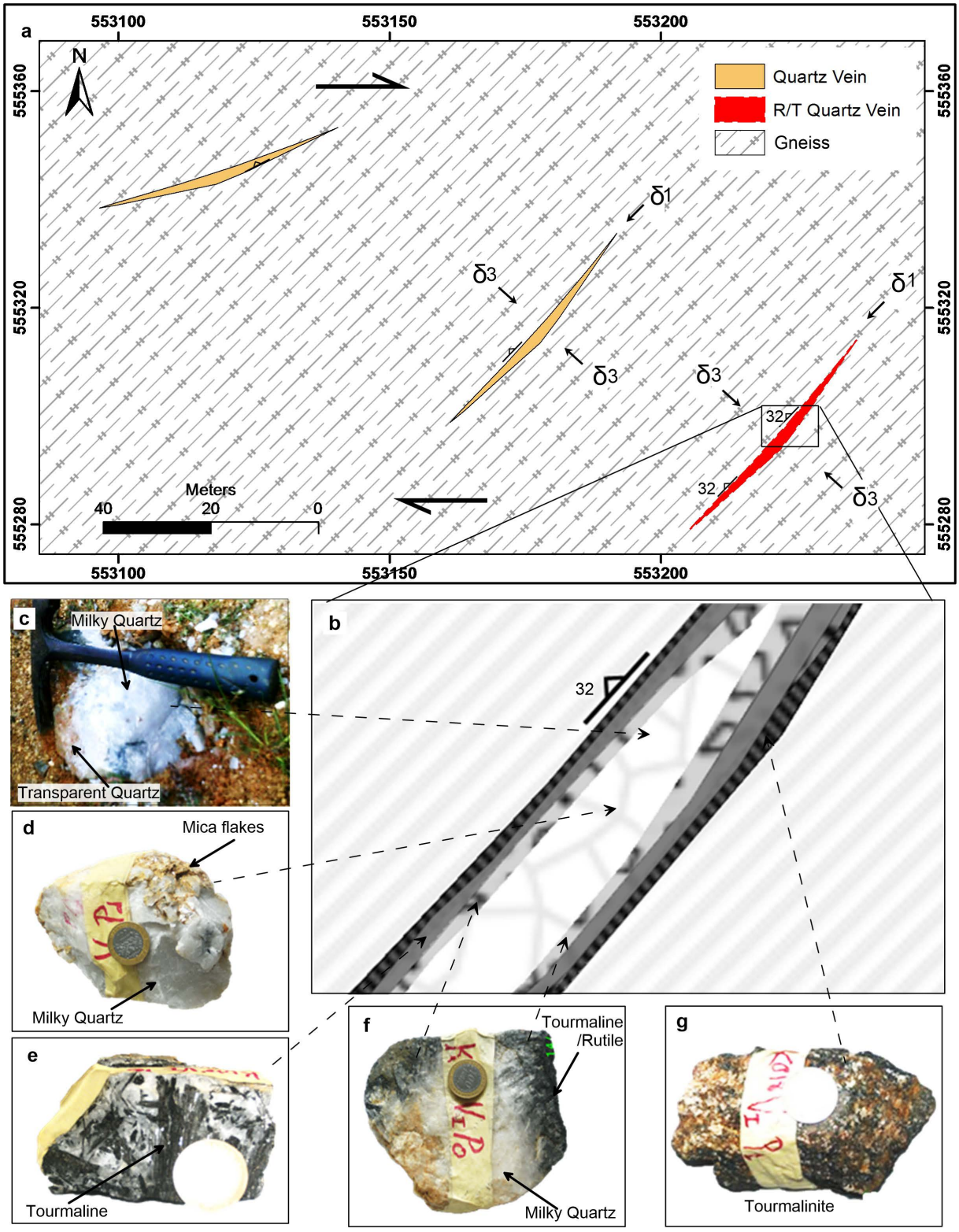

Figure 4. Field disposition and hand specimen features of quartzitic samples from the study area. (a) Structural vontext of some quartz veins in the Supe area with principal stress directions and shear indicators. (b) Well exposed vein with characteristic zonation and gradation from quartz in the core through mica flakes, tourmaline, and rutile inclusions in the rim. (c) Transparent to milky quartz with glassy to greasy luster. (d) Quartz occurring together with mica flakes. (e) Quartz with radiating dark rutile needles. (f) Quartz with dark tourmaline needles. (g) Tourmalinite.

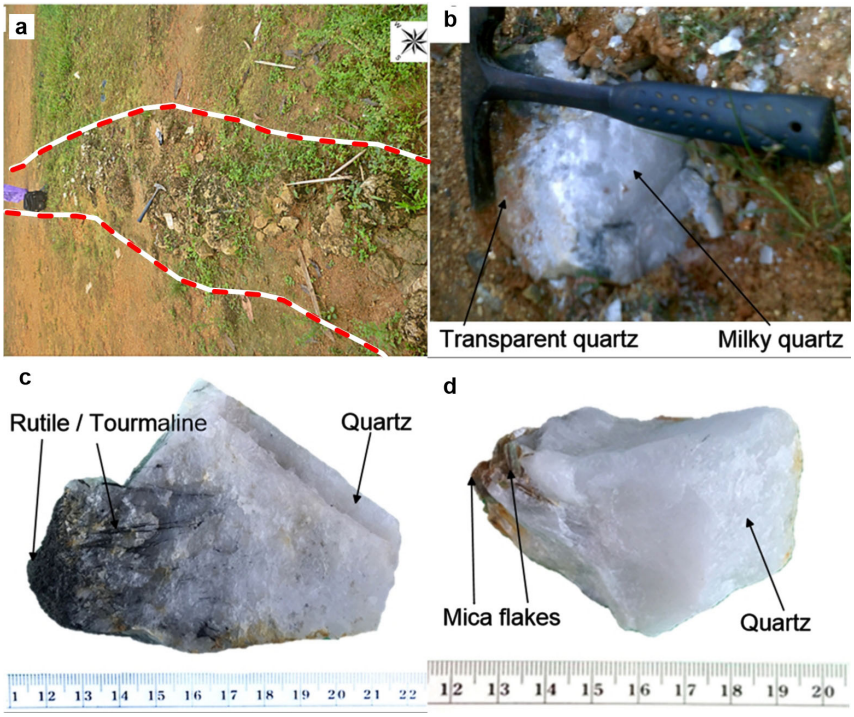

Figure 5. (a) and (b) Exposure of quartz-rich vein with a NE-SW trend exposed by erosion with the red-white dashed line marking the outline of the vein. (c) quartz-rich with rutile/tourmaline needles. (d) quartz with mica flakes.

of radiographs were acquired for one scan from different rotation angles between 0˚ and 360˚. Larger samples were scanned using a Hamamatsu L9181 tube set at 130 kV, 35 W source, with down to 5 μm spot size, because of its high power; smaller samples (resolution < 3 μm) were scanned with a Hamamatsu L1711 tube set at 100/160 kV (LaB6/W filament), 3 W, down to 400 nm spot size, because of its small spot size. The combination of both tubes covers all resolutions optimally, thus producing 2-D and 3-D images of the samples.

The chemical nature and other textural features of these samples were subsequently analyzed by scanning electron microscopy (SEM) and electron microprobe analysis (EMPA) [34] [35] at Activation Laboratory in Canada. Backscattered secondary electron images (BSE) were taken from inclusion-free quartz grains as well as from those with tourmaline/rutile inclusions. By a combination of image analysis employing atomic number contrast imaging (from back-scattered electron– or BSE-signal intensity) and Energy Dispersive Spectrometry (EDS) using Bruker 5010 SDD detectors, the tourmaline/rutile and quartz were directly measured through SEM. BSE signal intensity was proportional to the mean atomic number of the minerals. A Field Emission Gun was used at an accelerating voltage of 25 kV and a spot size of 5.5. ETD imaging was also used. Electron probe microanalysis measurements were performed in one analytical session where six quartz samples were analyzed as well as their tourmaline inclusions. These measurements were performed with a JEOL microprobe set at 15 kV, with a beam diameter of 5 μm.

4. Results

4.1. Petrography of Quartz Grains and Mineral Inclusions

2-D and 3-D images (Figure 6 and Figure 7) obtained by X-ray tomography as well as SEM/BSE images of quartz samples are used to describe the quartz textures. X-ray tomography images show two main minerals: quartz and rutile needles.

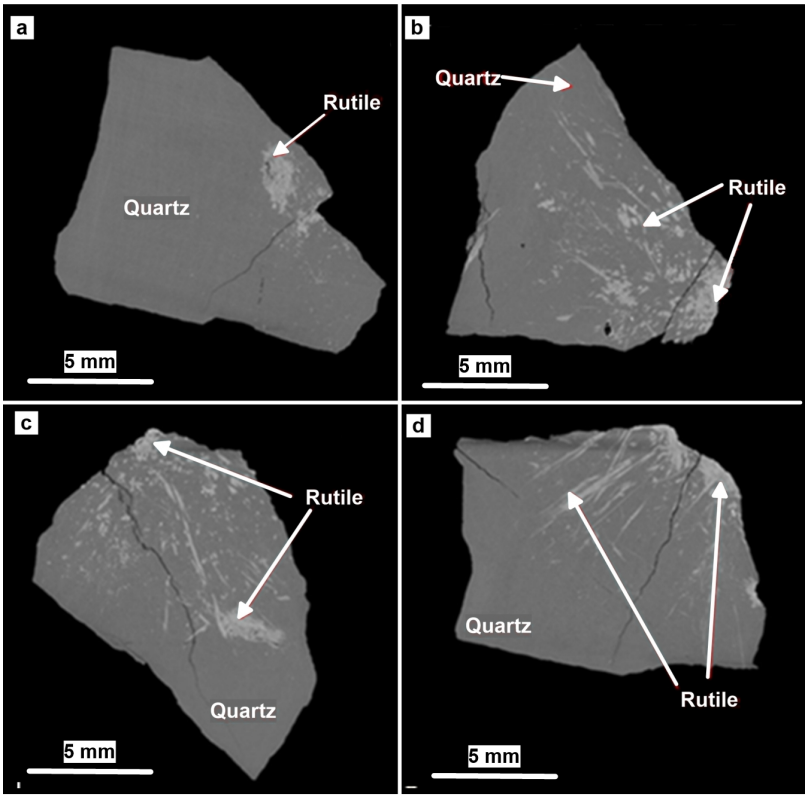

Figure 6. X-ray tomography 2-D images (a, b, c and d) of quartz crystals with fibrous rutile needles.

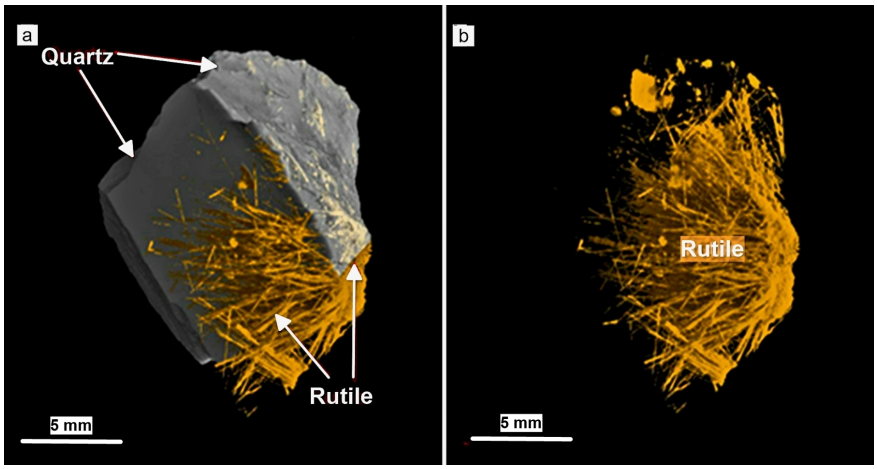

Figure 7. X-ray tomography 3-D images; (a) relationship between radiating fibrous rutile needles and quartz host. (b) Fibrous rutile needles only without quartz host, to emphasize the rutile texture.

In the 2-D images, the rutile needles appear to be disseminated as fibrous crystals within the quartz grains (Figure 6). The 3-D images better illustrate the relationship between the quartz crystals and rutile needles. The inclusions form radiating aggregates (Figure 7).

SEM images were obtained for both quartz and tourmaline crystals. The quartz grains are euhedral and large (2 - 3 mm) (Figure 8). Tourmaline is present in the quartz grains as inclusions (Figure 8(b) and Figure 8(c)). The tourmaline crystals are euhedral to subhedral with distinct perpendicular cleavages (Figure 9). Quartz makes up the matrix binding the tourmaline crystals together. However, rutile is also present in the tourmaline and quartz crystals (Figure 9(c)). The minerals show no zoning.

4.2. Microchemistry of Quartz and Tourmaline Inclusions

The quartz has a high amount of SiO_2 (>99.55%) and the other 9 oxides occupy < 0.5 weight % (Table 1).

The average weight percent of Ti is about 0.02, Al ≤ 0.01, and Fe, Mn, Mg, Cr and Ca. K and Na are between 0.01 - 0.07 wt%. These values have been converted to μg per gram (Table 1) and are compared with the average crustal values for quartz, HPQ, and IOTA standards (Figure 10).

Some elements such as Li, B, and P are below the detection limit. Al values generally fall within or below the three standards while Ti values are generally high in all but two samples where they are below the detection limit. The remaining elements are either high above all three standards or not detected at all. Al vs. the Ti concentrations for the quartz samples were determined and plotted

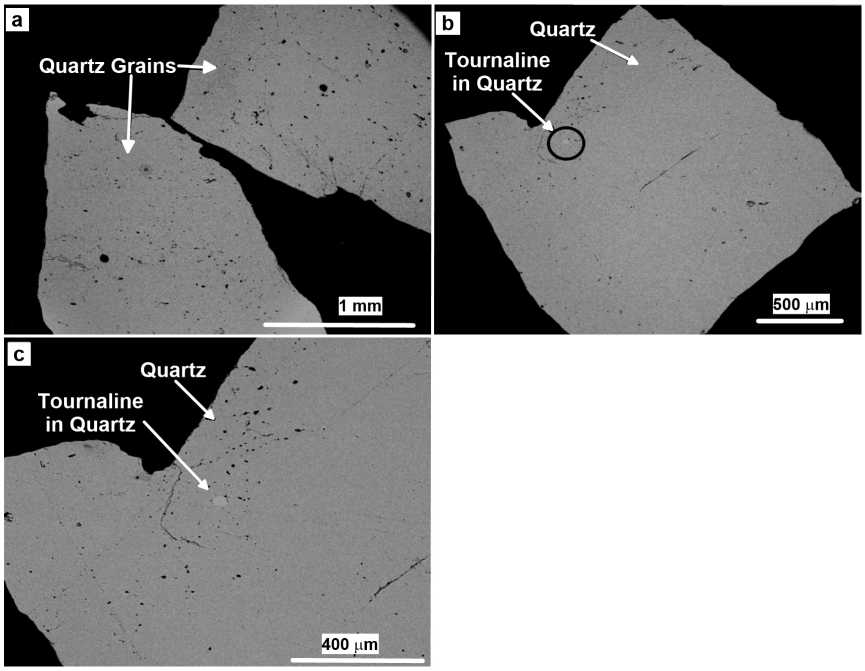

Figure 8. SEM images of (a) Quartz grains, (b), and (c) Quartz grains with tourmaline inclusions.

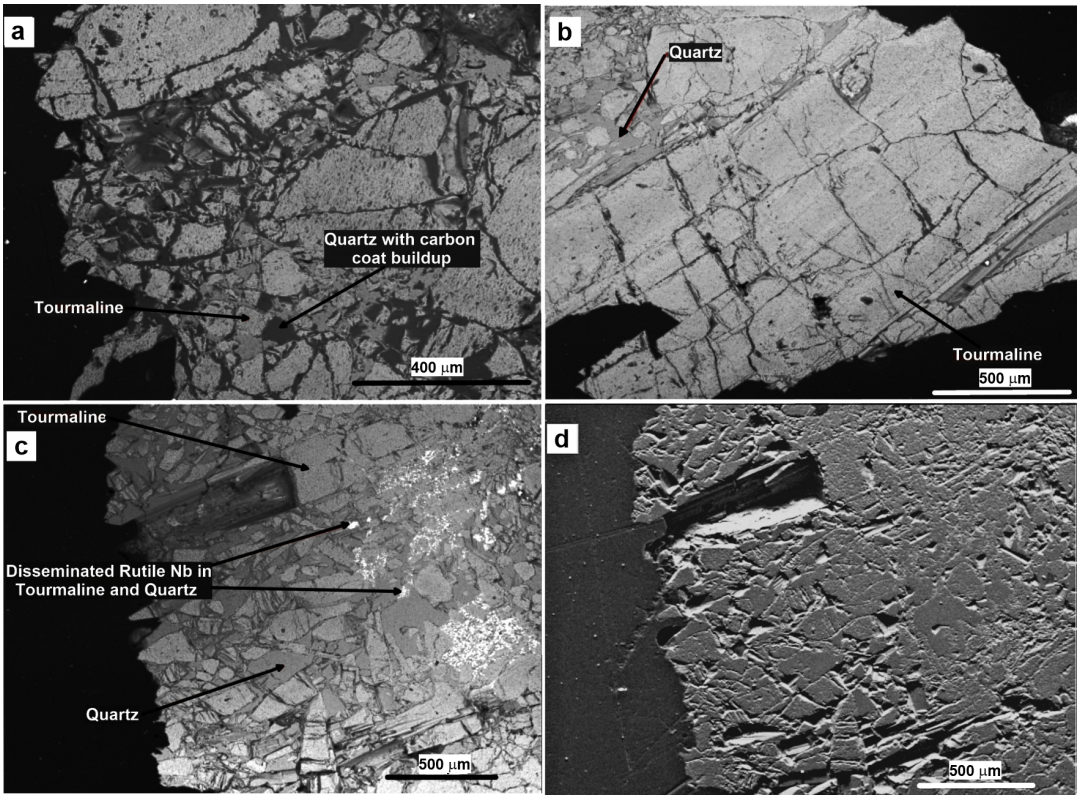

Figure 9. BSE image of tourmaline textures: (a) tourmaline in quartz matrix, (b) tourmaline selvages with distinct cleavages and fractures in quartz matrix, (c) disseminated rutile and Nb-bearing rutile phases in tourmaline and quartz crystals, (d) ETD BSE image showing the topography of disseminated rutile and Nb-bearing mineral in tourmaline and quartz crystals.

Table 1. Representative electron microprobe analysis data for quartz from vein samples in the Supe area.

	QTZ 1	QTZ 2	QTZ 3	QTZ 4	QTZ 5	QTZ 6	Average
SiO_2	99.99	100.11	99.98	100.30	99.55	99.85	**99.96**
TiO_2	0.04	0.01	0.00	0.09	0.05	0.00	**0.03**
Al_2O_3	0.00	0.00	0.02	0.01	0.02	0.00	**0.01**
FeO	0.02	0.00	0.00	0.03	0.04	0.00	**0.01**
MnO	0.00	0.00	0.00	0.00	0.11	0.00	**0.02**
MgO	0.01	0.02	0.05	0.01	0.03	0.00	**0.02**
CaO	0.01	0.02	0.01	0.00	0.01	0.01	**0.01**
Na_2O	0.04	0.00	0.01	0.00	0.01	0.00	**0.01**
K_2O	0.08	0.03	0.01	0.04	0.02	0.05	**0.04**
Cr_2O_3	0.05	0.01	0.00	0.00	0.00	0.00	**0.01**
Total	**100.25**	**100.20**	**100.08**	**100.47**	**99.83**	**99.91**	**100.12**
Wt%							
Si	46.99	47.05	46.99	47.14	46.79	46.93	**46.98**
Ti	0.02	0.00	0.00	0.05	0.03	0.00	**0.02**
Al	0.00	0.00	0.01	0.00	0.01	0.00	**0.00**

Continued

Fe	0.01	0.00	0.00	0.02	0.03	0.00	**0.01**
Mn	0.00	0.00	0.00	0.00	0.08	0.00	**0.01**
Mg	0.01	0.01	0.03	0.00	0.02	0.00	**0.01**
Ca	0.01	0.01	0.01	0.00	0.01	0.01	**0.01**
Na	0.03	0.00	0.01	0.00	0.01	0.00	**0.03**
K	0.07	0.03	0.01	0.03	0.01	0.04	**0.03**
Cr	0.03	0.01	0.00	0.00	0.00	0.00	**0.01**
µg per gram							
Si	469971.8	470498.2	469906	471405.3	467894.4	469285.6	**469826.88**
Ti	234.00	42.00	0.00	510.00	312.00	0.00	**183.00**
Al	10.60	10.60	100.70	37.10	79.50	5.30	**40.63**
Fe	156.00	0.00	0.00	234.00	273.00	0.00	**110.50**
Mn	0.00	0.00	0.00	0.00	847.00	0.00	**141.17**
Mg	84.00	90.00	306.00	48.00	180.00	0.00	**118.00**
Ca	71.00	142.00	71.00	0.00	71.00	71.00	**71.00**
Na	296.70	0.00	74.20	0.00	74.20	0.00	**318.17**
K	672.30	265.60	91.30	307.10	141.10	431.6	**318.17**
Cr	326.40	88.40	0.00	0.00	0.00	0.00	**69.13**

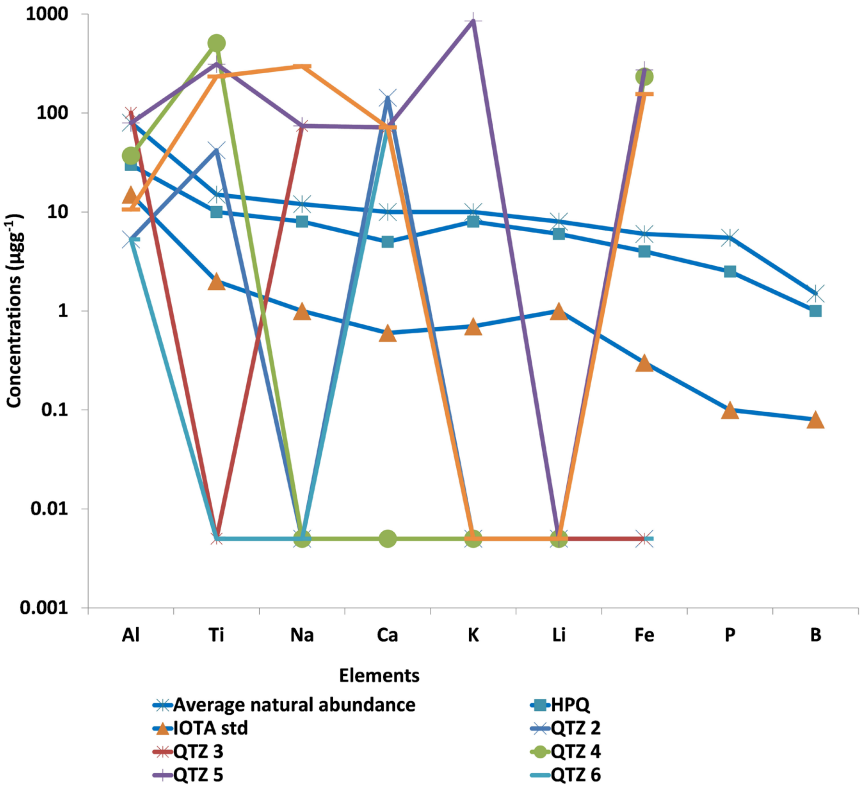

Figure 10. Microchemistry of quartz from Supe vein samples compared with the suggested upper concentration limits and average crustal abundance of nine detrimental trace elements in natural quartz of HPQ and the IOTA standard quartz [4].

to classify their purity levels. It appears that sample QTZ6 is of high purity, and that the other samples have low purity levels (Figure 11).

The microchemistry of tourmaline inclusions in the quartz (Table 2) shows high concentrations of SiO_2 (34.29 - 35.41 wt%) and Al_2O_3 (37.99 - 39.84 wt%) followed by FeO (5.32 - 8.58 wt%), MgO (4.48 - 7.16 wt%) and Na_2O (0.95 - 1.45 wt%), whereas most of the other oxides have concentrations ≤ 1 wt%. B, Li, and P are below the detection limit.

The cation numbers based on 30 oxygen were calculated and used to classify the tourmaline inclusions based on the generalized chemical formula for tourmaline which is $XY_3Z_6(T_6O_{18})$ $(BO_3)_3V_3$ W [38] where the most common ions (or vacancy) at each site are **X, Y, Z,** and **T**. These sites are defined as follows:

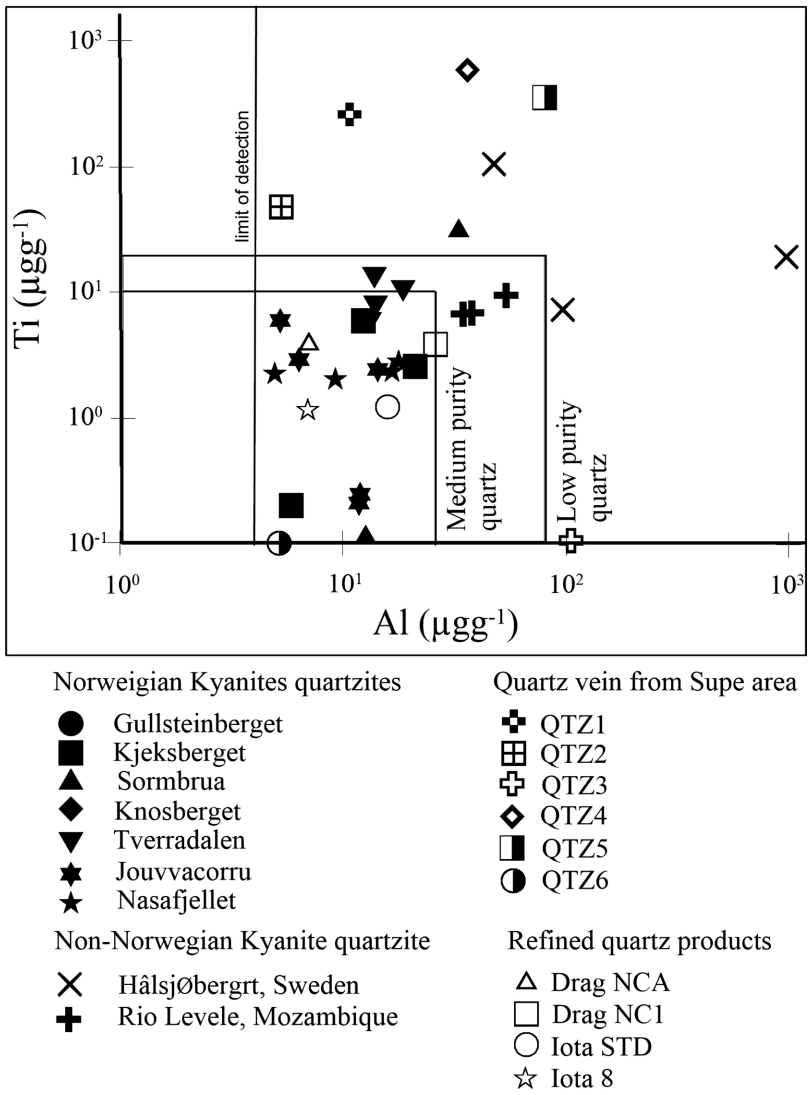

Figure 11. Al vs Ti plot of quartz microchemistry from the Supe vein, quartz in kyanite quartzites from Norway, Sweden, and Mozambique, and of refined HPQ products. Quartz with Al < 25 µg prer gram[1] and Ti < 10 µg oer gram is considered as "high-purity quartz". Concentrations of the quartz products Drag NC1, Drag NCA, Iota STD, and Iota 8 were analyzed by solution ICP-MS [5] [36].

Table 2. Electron microprobe analysis data for tourmaline inclusions in the Supe quartz vein samples.

	TOUR 1	TOUR 2	TOUR 3	TOUR 4	TOUR 5	TOUR 6
SiO_2	34.51	34.29	35.10	35.41	34.68	35.39
TiO_2	0.05	0.37	0.45	0.30	0.27	0.19
Al_2O_3	39.24	39.84	37.99	37.99	39.22	39.17
FeO	7.41	8.85	6.39	5.32	6.10	5.82
MnO	0.00	0.08	0.05	0.04	0.07	0.00
MgO	5.58	4.48	6.10	7.16	6.11	6.11
CaO	0.39	0.89	1.13	0.96	1.01	0.93
Na_2O	1.37	1.21	1.34	0.95	1.27	1.45
K_2O	0.05	0.03	0.05	0.03	0.05	0.05
P_2O_5	0.00	0.00	0.00	0.00	0.00	0.00
Total	**88.59**	**90.04**	**88.59**	**88.16**	**88.78**	**89.11**
Wt%						
Si	46.99	47.05	46.99	47.14	46.79	46.93
Ti	0.02	0.00	0.00	0.05	0.03	0.00
Al	0.00	0.00	0.01	0.00	0.01	0.00
Fe	0.01	0.00	0.00	0.02	0.03	0.00
Mn	0.00	0.00	0.00	0.00	0.08	0.00
Mg	0.01	0.01	0.03	0.01	0.01	0.00
Ca	0.01	0.01	0.00	0.00	0.01	0.00
Na	0.03	0.00	0.00	0.00	0.01	0.00
K	0.07	0.02	0.00	0.03	0.01	0.04316
Oxygens	2.57	2.59	2.58	2.59	2.59	2.61
F	12.04	11.95	12.01	11.97	11.96	11.88
Cation numbers based on 30 oxygen atoms						
Si	6.91	6.82	7.02	7.06	6.90	6.99
Ti	0.01	0.05	0.07	0.04	0.04	0.03
Al	9.26	9.34	8.95	8.92	9.20	9.13
Fe	1.24	1.47	1.07	0.89	1.02	0.96
Mn	0.00	0.01	0.01	0.01	0.01	0.00
Mg	1.67	1.33	1.82	2.13	1.81	1.80
Ca	0.08	0.19	0.24	0.20	0.22	0.19
Na	0.53	0.47	0.52	0.37	0.49	0.56
K	0.01	0.01	0.02	0.01	0.01	0.01
Total	**19.72**	**19.69**	**19.72**	**19.63**	**19.71**	**19.69**
X site	0.63	0.67	0.78	0.58	0.72	0.77
Y site	2.91	2.87	2.96	3.06	2.88	2.79
Z site						
T site	8.44	9.44	10.44	11.44	12.44	13.44

X = Na^{1+}, Ca^{2+}, $K1^{+}$, and vacancy, **Y** = Fe^{2+}, Mg^{2+}, Mn^{2+}, Al^{3+}, Li^{1+}, Fe^{3+}, and Cr^{3+}

Z = Al^{3+}, Fe^{3+}, Mg^{2+}, and Cr^{3+} **T** = Si^{4+}, Al^{3+}, and B^{3+}

B = B^{3+}; V = OH^{1-} and O^{2-} **W** = OH^{1-}, F^{1-}, and O^{2-}.

Most compositional variability occurs at the **X, Y, Z, W**, and **V** sites. Tourmaline species are defined following the dominant-valency rule such that in a relevant site the dominant ion of the dominant valence state is used for the basis of nomenclature [39] thus classifying the tourmaline as shown in **Table 3**.

5. Interpretation and Discussion

5.1. Structural Configuration of the Supe Area

Quartz veins with a similar orientation as in the Supe area (N32E) have been reported from the Betare Oya District [40] where they form part of the Lom Series with strike values between N30E-N40E [13]. These veins are rather lode gold-bearing and are concordant with the regional foliations of the area. NE-SW-trending sinistral wrench movements have been reported for this area [41] which controls the gold mineralization. The orientation of the quartz veins of the Supe area as well as those of the Betare Oya District therefore all form part of the CCSZ (N30E-N70E) lineament, which is a segment of the CASZ [13] [17].

5.2. HPQ Economic Potential of the Supe Area

Synthetic quartz is a raw material for special applications in high-tech industries, but it has a high cost of production. To meet up with the high demand and also to minimize cost, attention has shifted worldwide to natural quartz which, however, naturally occurs with impurities that affect the quality of its products.

Very high purity quartz for advanced high-tech applications is currently sourced from only a few locations around the world. The expected growth in demand implies that more sources have to be found and this is what contributed to the interest in the Supe veins. Of the nine determinant trace elements used to classify HPQ [35], three (Li, P, and B) are below the detection limit; Al concentrations are within the HPQ, IOTA, and average natural abundance; Ti values are high

Table 3. Nomenclature of tourmaline types in quartz vein samples from the Supe area.

	X	Y_3	Z_6	V_3	Names
TOUR 1	Na	Fe^{3+}	Al	OH^{1-}	Schorlitic tourmaline
TOUR 2	Na	Mg	Al	OH^{1-}	Dravitic tourmaline
TOUR 3	Na	Mg	Al	OH^{1-}	Dravitic tourmaline
TOUR 4	Na	Fe^{3+}	Al	OH^{1-}	Schorlitic tourmaline
TOUR 5	Na	Fe^{3+}	Al	OH^{1-}	Schorlitic tourmaline
TOUR 6	Na	Fe^{3+}	Al	OH^{1-}	Schorlitic tourmaline

General formula: Schorlite = $(NaCa)Fe_3(Al,Fe)_6[Si_6O_{18}][BO_3](OH,F)_4$; Dravite = $NaMg_3(Al,Fe)_6[Si_6O_{18}][BO_3](OH,F)_4$.

above all three standards in all except one sample, while Na, Ca, K, and Fe values fluctuate (**Figure 10**) thus classifying QTZ6 as high purity quartz, purer than the Norweigian kyanite quartzites as well as the refined quartz products. The other samples were classified as low purity (**Figure 11**), similar to the Hålsjøberget kyanite quartzites of Sweden [35] except for their lower Al concentration, as well as to the Serra de Santa Helena quartz resource, Brazil, with a relatively low Al content of about 15 μg per gram[1] [8].

The presence of rutile, tourmaline, and mica inclusions in the samples from the Supe veins affects the purity of the quartz. However, the quartz can be processed in four different stages according to [2]: pre-processing (mechanical crushing, required to liberate mineral impurities and fluid inclusions for further physical treatment), physical processing (attrition, magnetic separation, and high tension separation flotation), chemical leaching, and thermal treatment. Also the random distribution of inclusions in portions within the vein, the large grain sizes and density contrasts, straight and planar grain boundaries, absence of intergrowths, and grain boundary migration help in the refining process for easy sorting of optically pure portions which require less treatment and easy elimination of mineral inclusions. The low level of certain impurities in the Supe quartz veins suggests that it is feasible to give metallurgical treatment to the quartz of this area to obtain HPQ.

These veins define tension gashes which usually occur in an en-echelon arrangement covering a large surface area. This is strong evidence that more of such veins exist in the Supe area. Also, the occurrence of quartzitic bodies of hydrothermal origin in the Neoproterozoic Braziliano belt [8] of South America indicates the possibility of such bodies in that area. Thus, combining the possible quantities and quality, this area is a promising deposit for HPQ industries for the manufacture of low- to high-purity quartz products.

5.3. Origin of the Inclusions in the Quartz Vein

The inclusions in this study include tourmaline (primarily schorlite), rutile, and mica flakes which all occur as macro- to micro-inclusions down to <1 μm. Among these minerals, rutile often occurs in association with other phases in hydrothermal vein systems, thus providing using rutile thermometry [42] and [43] information about the origin, mode of formation, and possible ages. The formation of mineral inclusions in quartz is manifold [44]. According to [35], all mineral phases which occur in the host rock may also occur as micro-inclusions in quartz, and they were enclosed during growth from melt and fluids or by solid-state grain-boundary migration during metamorphism and subsequent crystal lattice recovery, which is very common in metamorphic rocks like quartzite.

Rutile in the Supe quartz veins has two possible origins; it could have formed during vein crystallization within the quartz crystals or secondary, due to hydrothermal alteration (chloritisation) of Ti-rich biotite [45]. The rutile and mica in these veins may have originated from hydrothermal processes affecting the

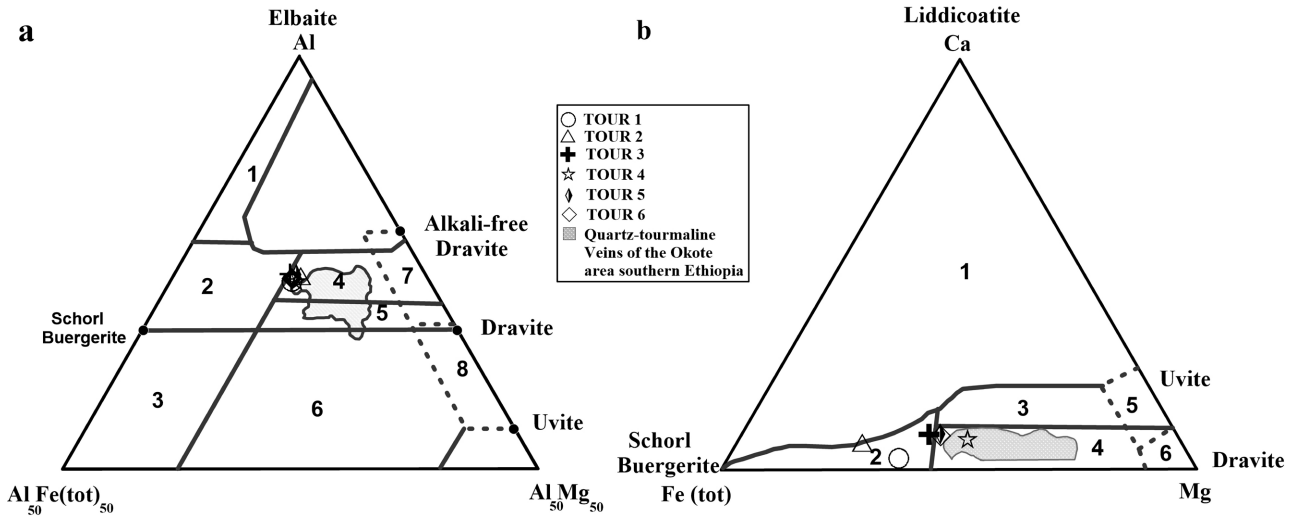

Figure 12. Classification of the chemical composition of tourmaline in the Supe quartz veins compared with the quartz-tourmaline veins of the Okote area, southern Ethiopia (in gray) using ternary diagrams of [37]. (a) Al-Fe (tot)-Mg diagram. Fields 1 = Li-rich granitoids, pegmatites; 2 = Li-poor granitoids and their pegmatites, and aplites; 3 = Fe^{3+}-rich quartz-tourmaline rocks (hydrothermally altered granites); 4 = Metapelites and meta-psammites, with Al-saturated phase; 5 = Metapelites and metapsammites without Al-saturated phase; 6 = Fe^{3+}-rich quartz-tourmaline rocks, calc-silicate rocks and metapelites; 7 = Low Ca meta-ultramafic and Cr, V-rich meta-sediments; 8 = Metacarbonates and metapyroxenites (b) Ca-Fe(tot)-Mg diagram: Fields 1 = Li-rich granitoids, pegmatites and aplites; 2 = Li-poor granitoids and their pegmatites, and aplites; 3 = Ca-rich metapelites, meta-psammites, and calc-silicate rocks; 4 = Ca-poor metapelites, metapsamnites, and calc-silicate rocks; 5 = metacarbonates; 6 = meta-ultramafics.

wall/host rocks [35], which are gneisses. The gneisses are rich in rutile that is strongly associated with biotite so that decompression during tectonic uplift and cooling may be responsible for the development of the rutile needles as inclusions in the quartz [46] [47].

The tourmaline crystals in the Supe veins are of hydrothermal origin with a metamorphic overprint. Such metamorphic effects on hydrothermal tourmaline have been described by [48] (**Figure 12**), which favors meta-sedimentary rocks as the main source.

6. Conclusion

The following conclusions can be drawn from this study. The tourmaline inclusions have a hydrothermal origin with a metamorphic overprint while the rutile and micas might have a primary or secondary origin. A primary origin could have formed during vein crystallization within the quartz crystals (exsolution) as a result of decompression during tectonic uplift and cooling, or secondary due to hydrothermal extraction into the veins. The Supe quartz veins are metamorphic/hydrothermal in origin. The quality and quantity of the HPQ veins in this area suggest a high potential for HPQ exploration in the region.

Acknowledgements

The data presented are from parts of Arnold Chi Kedia's master thesis supervised by Cheo Emmanuel Suh and supplemented by Afahnwie Ngambu Aloysius and Cyrille Sigue. Financial supports from coordinated institutional that grants

to Elisha Mutum Shemang and Cheo Emmanuel Suh are acknowledged. The authors acknowledge support from colleagues at the University of Buea and the Remote Sensing Unit.

Conflicts of Interest

The authors declare no conflict of interest.

References

[1] Müller, A., Ihlen, P.M., Wanvik, J.E. and Flem, B. (2007) High-Purity Quartz Mineralisation in Kyanite Quartzites, Norway. *Mineralium Deposita*, **42**, 523-535. https://doi.org/10.1007/s00126-007-0124-8

[2] Haus, R., Prinz, S. and Priess, C. (2012) Assessment of High Purity Quartz Resources. In: Götze, J. and Möckel, R., Eds., *Quartz: Deposits, Mineralogy and Analytics*, Springer, Heidelberg, 29-51. https://doi.org/10.1007/978-3-642-22161-3_2

[3] SINOSI Group. http://www.sinosi.com

[4] High Purity Quartz Market Insights, 2031 https://www.transparencymarketresearch.com/high-purity-quartz-market.html

[5] Norwegian Crystallites AS. Norwegian Crystallites AS-Products-Crystal Quartz Analyses. http://www.norcryst.no

[6] Haus, R. (2005) High Demands on High Purity. *Industrial Minerals*, **10**, 62-67.

[7] Haus, R. (2010) High-Purity Quartz Resources. *Proceedings of the PHOTON's 8th Solar Silicon Conference*, Stuttgart, 27 April 2010.

[8] Santos, F.M., Fujiwara, E., Schenkel, E.A., Enzweiler, J. and Suzuki, K.C. (2014) Quartz Resource in the Serra de Santa Helena Formation, Brazil: A Geochemical and Technological Study. *Journal of South American Earth Sciences*, **56**, 328-338. https://doi.org/10.1016/j.jsames.2014.09.017

[9] Harben, P.W. (2002) The Industrial Mineral Handy Book—A Guide to Markets, Specifications and Prices. 4th Edition, Industrial Mineral Information, Worcester Park.

[10] Kedia, A.C. (2011) The Geology of Supe and Its Environs, GLY 498 Project. University of Buea, Cameroon.

[11] Njome, M.S. (2000) Structural Features of the Migmatite-Gneiss/Mylonite Association of the Tombel Graben, South Western Cameroon. University of Buea, Cameroon.

[12] Njome, M.S., Suh, C.E, and Ghogomu, R.T. (2000) A Micro Structural Approach to Interpreting the Structural Setting of the Tombel Graben, South Western Cameroon. *GeoActa*, **2**, 181-200.

[13] Sigue, C., Moundi, A., Suh, C.E., dos Santos, M.F.M., Fujiwara, E., Suzuki, C.K. and Ndema-Mbongue, J.L. (2020) Assessment of Shear Zone-Derived Quartz from the Etam Area, Southwest Cameroon as Potential High-Purity Quartz Resource: Petrography, Geochemistry and Technological Studies. *Carlos Kenichi Suzuki*, **2**, Article No. 551. https://doi.org/10.1007/s42452-020-2301-7

[14] Toteu, S., Van Schmus, W., Penaye, J. and Michard, A. (2001) New U–Pb and Sm–Nd Data from North-Central Cameroon and Its Bearing on the Pre-Pan African History of Central Africa. *Precambrian Research*, **108**, 45-73. https://doi.org/10.1016/S0301-9268(00)00149-2

[15] Ngako, V., Affaton, P. and Njonfang, E. (2008) Pan-African Tectonics in North-

western Cameroon: Implication for the History of Western Gondwana. *Precambrian Research*, **14**, 509-522. https://doi.org/10.1016/j.gr.2008.02.002

[16] Ngako, V., Affaton, P., Nnange, J.M. and Njanko, T. (2003) Pan-African Tectonic Evolution in Central and Southern Cameroon: Transpression and Transtension during Sinistral Shear Movements. *Journal of African Earth Sciences*, **36**, 207-214. https://doi.org/10.1016/S0899-5362(03)00023-X

[17] Njome, M.S. and Suh, C.E. (2005) Tectonic Evolution of the Tombel Graben Basement, Southwestern Cameroon. *Episodes*, **28**, 37-41. https://doi.org/10.18814/epiiugs/2005/v28i1/004

[18] Kamdem, J.B., Kraml, M., Keller, J. and Henjes-Kunst, F. (2002) Cameroon Line Magmatism: Conventional K/Ar and Single-Crystal Laser $^{40}Ar/^{39}Ar$ Ages of Rocks and Minerals from the Hossere Nigoanorogenic Complex, Cameroon. *Journal of African Earth Sciences,* **35**, 99-101. https://doi.org/10.1016/S0899-5362(02)00002-7

[19] Suh, C.E. and Lehmann, B. (2003) Morphology and Electron-Probe Microanalysis of Residual Gold-Grains at Dimako, Southeast Cameroon. *Neues Jahrbuch für Mineralogie*, *Monatshefte*, **2003**, 255-275. https://doi.org/10.1127/0028-3649/2003/2003-0255

[20] Montigny, R., Ngounouno, I. and Deruelle, B. (2004) Ages K-Ar des roches magmatiques du fosse de Garoua (Cameroun): Leur place dans le cadre de la ligne du Camerounî. *Comptes Rendus Geoscience,* **336**, 1463-1471. https://doi.org/10.1016/j.crte.2004.08.005

[21] Nkouathio, D. (1997) Le volcanisme recent du graben de Tombel (province du littoral et du sud-ouest, Cameroun): Volcanologie, geochimie, petrologie et valeuragricole. Universite de Yaounde I, Cameroun.

[22] Lamilen, B.D., Moundi, A., Moupou, M. and Minyem, D. (1998) Control structurel du socledans la morphologie du massif anorogenique du Koupe (Ligne du Cameroun). *Geosci. au Cameroun*, **1**, 191-196.

[23] Aka, F.T. (2009) Volcanism along the Cameroon Volcanic Line. *Journal of African Earth Sciences*, **55**, 175-184. https://doi.org/10.1016/j.jafrearsci.2009.04.002

[24] Djouka-Fonkwe, M.L., Schulz, B., Schüssler, U., Tchouankoué, J.P. and Nzolang, C. (2008) Geochemistry of the Bafoussam Pan-African I- and S-Type Granitoids in Western Cameroon. *Journal of African Earth Sciences*, **50**, 148-167. https://doi.org/10.1016/j.jafrearsci.2007.09.015

[25] De Witt, J., Stankiewicz, J. and Reeves, C. (2008) Restoring Pan-African-Brasiliano Connections: More Gondwana Control, Less Trans-Atlantic Connetion. *Geological Society*, *London*, *Special Publications*, **294**, 399-412. https://doi.org/10.1144/SP294.20

[26] Njiekak, G., Dörr, W., Tchouankoué, J.-P. and Zulauf, G. (2008) U–Pb Zircon and Microfabric Data of (Meta) Granitoids of Western Cameroon: Constraints on the Timing of Pluton Emplacement and Deformation in the Pan-African Belt of Central Africa. *Lithos*, **102**, 460-477. https://doi.org/10.1016/j.lithos.2007.07.020

[27] Mosoh Bambi, C.K., Suh, C.E., Nzenti, J.P. and Frimmel, H.E. (2012) UMo Mineralization Potential in Pan-African Granites, Southwestern Cameroon: Economic Geology of the Ekomédion PROSPECT. *Journal of African Earth Sciences*, **65**, 25-45. https://doi.org/10.1016/j.jafrearsci.2012.01.001

[28] Mosoh Bambi, C.K., Frimmel, H.E., Zeh, A., Suh, C.E. (2013) Age and origin of Pan-African Granites and Associated U–Mo Mineralization at Ekomédion, Southwestern Cameroon. *Journal of African Earth Sciences*, **88**, 15-37. https://doi.org/10.1016/j.jafrearsci.2013.08.005

[29] Kouske, A.P., Suh, C.E., Ghogomu, R.T. and Ngako, V. (2012) Na-Metasomatism and Uranium Mineralization during a Two-Stage Albitization at Kitongo, Northern Cameroon: Structural and Geochemical Evidence. *International Journal of Geosciences*, **3**, 258-279. https://doi.org/10.4236/ijg.2012.31028

[30] Suh, C.E., Lehmann, B. and Mafany, G.T. (2006) Geology and Geochemical Aspects of Lode Gold Mineralization at Dimako-Mboscorro, SE Cameroon. *Geochemistry: Exploration, Environment, Analysis*, **6**, 295-309. https://doi.org/10.1144/1467-7873/06-110

[31] Fon, N. (2006) Tourmalinization in the Betare Oya Gold District East Cameroon Gold Field. University of Buea, Cameroon.

[32] Kyle, J.R., Mote, A.S. and Ketcham, R.A. (2008) High Resolution X-Ray Computed Tomography Studies of Grasberg Porphyry Cu-Au Ores, Papua, Indonesia. *Mineralium Deposita*, **43**, 519-532. https://doi.org/10.1007/s00126-008-0180-8

[33] Mees, F., Swennen, R., Geet, M. and Van Jacobs, P. (2003) Applications of X-Ray Computed Tomography in the Geosciences. *Geological Society, London, Special Publications*, **215**, 1-6. https://doi.org/10.1144/GSL.SP.2003.215.01.01

[34] Müller, A., Herrington, R., Armstrong, R., Seltmann, R., Kirwin, D.J., Stenina, N.G. and Kronz, A. (2010) Trace Elements and Cathodoluminescence of Quartz in Stockwork Veins of Mongolian Porphyry-Style Deposits. *Mineralium Deposita*, **45**, 707-727. https://doi.org/10.1007/s00126-010-0302-y

[35] Müller, A., Wanvik, J.E. and Ihlen, P.M. (2012) Petrological and Chemical Characterisation of High-Purity Quartz Deposits with Examples from Norway. In: Götze, J. and Möckel, R., Eds., *Quartz: Deposits, Mineralogy and Analytics*, Springer, Berlin, Heidelberg, 71-118. https://doi.org/10.1007/978-3-642-22161-3_4

[36] Moore, P. (2005) High-Purity Quartz. *Industrial Minerals*, **455**, 53-57.

[37] Henry, D.J. and Guidotti, C.V. (1985) Tourmaline as a Petrogenetic Indicator Mineral: An Example from the Staurolite-Grade Metapelites of NW Maine. *American Mineralogist,* **70**, 1-15.

[38] Hawthorne, F.C. and Henry, D.J. (1999) Classification of the Minerals of the Tourmaline Group. *European Journal of Mineralogy*, **11**, 201-215. https://doi.org/10.1127/ejm/11/2/0201

[39] Henry, D.J., Novák, M.C., Hawthorne, F.C., Ertl, A., Dutrow, B.L., Uher, P. and Pezzotta, F. (2011) Nomenclature of the Tourmaline-Super Group Minerals. *American Mineralogist*, **96**, 895-913. https://doi.org/10.2138/am.2011.3636

[40] Suh, C.E., Cabral, A.R., Shemang, E.M., Mbinkar, L. and Mboudou, G.G.M. (2008) Two Contrasting Iron Deposits in the Precambrian Mineral Belt of Cameroon, West Africa. *Exploration and Mining Geology*, **17**, 197-207. https://doi.org/10.2113/gsemg.17.3-4.197

[41] Ngako, V., Njonfang, E., Aka, F.T., Affaton, P., Nnange, J.M. (2006) The North-South Paleozoic to Quaternary Trend of Alkaline Magmatism from Niger-Nigeria to Cameroon: Complex Interaction between Hotspots and Precambrian faults. *Journal of African Earth Sciences*, **45**, 241-256. https://doi.org/10.1016/j.jafrearsci.2006.03.003

[42] Meinhold, G., Anders, B., Kostopoulos, D. and Reischmann, T. (2008) Rutile Chemistry and Thermometry as Provenance Indicator: An Example from Chios Island, Greece. *Sedimentary Geology,* **203**, 98-111. https://doi.org/10.1016/j.sedgeo.2007.11.004

[43] Meinhold, G. (2010) Rutile and Its Applications in Earth Sciences. *Earth-Science Reviews,* **102**, 1-28. https://doi.org/10.1016/j.earscirev.2010.06.001

[44] Götze, J. (2010) Chemistry, Textures and Physical Properties of Quartz Geological Interpretation and Technical Application. *Mineralogical Magazine*, **3**, 645-671. https://doi.org/10.1180/minmag.2009.073.4.645

[45] Carruzzo, S., Clarke, D.B., Pelrine, K.M. and MacDonald, M.A. (2006) Texture, Composition, and Origin of Rutile in the South Mountain Batholith, Nova Scotia. *The Canadian Mineralogist,* **44**, 715-729. https://doi.org/10.2113/gscanmin.44.3.715

[46] Cherniak, D.J., Watson, E.B. and Wark, D.A. (2007) Ti Diffusion in Quartz. *Chemical Geology*, **236**, 65-74. https://doi.org/10.1016/j.chemgeo.2006.09.001

[47] Adachi, T., Hokada, T., Osanai, Y., Toyoshima, T., Baba, S. and Nakano, N. (2010) Titanium Behavior in Quartz during Retrograde Hydration: Occurrence of Rutile Exsolution and Implications for Metamorphic Processes in the Sør Rondane Mountains, East Antarctica. *Polar Science,* **3**, 222-234. https://doi.org/10.1016/j.polar.2009.08.005

[48] Deksissa, D.J. and Koeberl, C. (2002) Geochemistry and Petrography of Gold-Quartz-Tourmaline Veins of the Okote Area, Southern Ethiopia: Implications for Gold Exploration. *Mineralogy and Petrology*, **75**, 101-122. https://doi.org/10.1007/s007100200018